Hindawi
Contrast Media & Molecular Imaging
Volume 2021, Article ID 8988762, 8 pages
https://doi.org/10.1155/2021/8988762

Research Article

GlyCEST: Magnetic Resonance Imaging of Glycine—Distribution in the Normal Murine Brain and Alterations in 5xFAD Mice

Ken Ohno,[1,2] **Masaki Ohkubo**,[3] **Bingwen Zheng**,[4] **Masaki Watanabe**,[1] **Tsuyoshi Matsuda**,[5] **Ingrid L. Kwee**,[6] **and Hironaka Igarashi**[1]

[1]*Center for Integrated Human Brain Science, Brain Research Institute, University of Niigata, Niigata 951-8585, Japan*
[2]*Department of Radiological Technology, Faculty of Medical Technology, Niigata University of Health and Welfare, Niigata 950-3198, Japan*
[3]*Department of Radiological Technology, School of Health Sciences, Faculty of Medicine, University of Niigata, Niigata 951-8518, Japan*
[4]*Time Medical Ltd., Hong Kong Science & Technology Park, Hong Kong, China*
[5]*Division of Ultrahigh Field MRI, Institute for Biomedical Sciences, Iwate Medical University, Iwate 028-3694, Japan*
[6]*Department of Neurology, University of California Davis, CA 94553, USA*

Correspondence should be addressed to Hironaka Igarashi; higara@bri.niigata-u.ac.jp

Received 16 August 2021; Accepted 14 December 2021; Published 30 December 2021

Academic Editor: Pedro Rosa-Neto

The glycine level in the brain is known to be altered in neuropsychiatric disorders, such as schizophrenia and Alzheimer's disease (AD). Several studies have reported the *in vivo* measurement of glycine concentrations in the brain using proton magnetic resonance spectroscopy (^{1}H-MRS), but ^{1}H-MRS is not capable of imaging the distribution of glycine concentration with high spatial resolution. Chemical exchange saturation transfer magnetic resonance imaging (CEST-MRI) is a new technology that can detect specific molecules, including amino acids, in tissues. To validate the measurements of glycine concentrations in living tissues using CEST from glycine to water (GlyCEST), we extracted the brain tissues from mice and performed biochemical tests. In wild-type C57BL/6 mice, GlyCEST effects were found to be higher in the thalamus than in the cerebral cortex ($P < 0.0001$, paired t-test), and this result was in good agreement with the biochemical results. In 5xFAD mice, an animal model of AD, GlyCEST measurements demonstrated that glycine concentrations in the cerebral cortex ($P < 0.05$, unpaired t-test) and thalamus ($P < 0.0001$, unpaired t-test), but not in the hippocampus, were decreased compared to those in wild-type mice. These findings suggest that we have successfully applied the CEST-MRI technique to map the distribution of glycine concentrations in the murine brain. The present method also captured the changes in cerebral glycine concentrations in mice with AD. Imaging the distribution of glycine concentrations in the brain can be useful in investigating and elucidating the pathological mechanisms of neuropsychiatric disorders.

1. Introduction

Glycine, which is the simplest amino acid found in the proteins of living organisms, is known to act as an inhibitory neurotransmitter in the brainstem and spinal cord of the central nervous system [1, 2]. In contrast, it acts in the cerebrum as a coagonist for the N-methyl-D-aspartate (NMDA) receptor, an ionotropic glutamate receptor [3, 4]. The NMDA receptor controls the influx of calcium into neurons and is essential for synaptic transmission, neuroplasticity, and learning and memory mechanisms [5, 6]. Activation of NMDA receptors requires the binding of glutamate and glycine to their binding sites in their respective subunits [7]. The extracellular glycine concentration is altered by brain activity and is mainly regulated by astrocytic glycine transporters [8]. Glycine concentration is

thought to be related to NMDA receptor function, and glycine is sometimes used for the treatment of schizophrenia [9]. Considering the essential roles of glycine in brain metabolism and function, better knowledge about glycine distribution *in vivo* may further elucidate its functions under physiological and pathological conditions.

The glycine concentration in the brain is known to be altered in neuropsychiatric disorders such as schizophrenia and Alzheimer's disease (AD) [10–12]. In patients with AD, blood and brain glycine concentrations differ from those in healthy subjects [10, 11], although other studies have shown that glycine concentrations are unchanged in patients with AD [12]. We hypothesized that these inconsistent data could be caused by variations in glycine concentrations in the different areas of the brain. Thus, the measurement of regional glycine concentrations and imaging of glycine concentration distributions in the brain may provide knowledge on the pathogenesis of AD and facilitate the staging of this disease.

To measure the concentration of glycine in living tissues, it is necessary to extract the tissues and measure the amount of protein using high-performance liquid chromatography (HPLC) or mass spectroscopy. Several studies have reported the *in vivo* measurement of glycine concentrations in the brain using proton magnetic resonance spectroscopy (^{1}H-MRS) [13–15], but this technique is not capable of showing the glycine concentration distribution with high spatial resolution. Chemical exchange saturation transfer magnetic resonance imaging (CEST-MRI), which measures the exchange of target metabolite protons to water molecules and calculates the concentration of metabolites [16], can be used to obtain the glycine concentration distribution with high spatial resolution.

The purpose of this study was to establish a method to measure the distribution of glycine using the CEST-MRI technique (GlyCEST) and evaluate the application of this method in diseases. We first validated GlyCEST using a phantom containing solutions of known glycine concentrations. Subsequently, we applied the method to the murine brain *in vivo*. Finally, the 5xFAD mouse model of AD [17] was used to verify the capability of this method to detect changes in glycine concentrations in the brains of mice with AD.

2. Materials and Methods

2.1. Phantom Preparation. To study the linearity of concentration-dependent GlyCEST effects, we used solutions with varying glycine concentrations (0, 2.5, 5.0, 7.5, and 10.0 mM) in phosphate-buffered saline, adjusted to pH 7.0 using 1 M HCl or 1 M NaOH. These solutions were added to 10.8 mm inner diameter tubes that were immersed in a 33.7 mm inner diameter glass tube filled with phosphate-buffered saline at pH 7.0.

2.2. Experimental Animals and Setup. This study was approved by the Institutional Animal Care and Use Committee of Niigata University (SA00849) and conducted in accordance with the Guidelines of the US National Institutes of Health regarding the care and use of animals for experimental procedures [18]. We utilized seven homozygous 5xFAD transgenic male mice expressing five mutant human genes associated with AD (APPSwFlLon, PSEN1*M146L*L286V) and 6799Vas/Mmjax [17] at 16-17 months of age, as well as 16 C57BL/6 wild-type (WT) male mice at 2-3 months of age. Breeding progenitors were purchased from Jackson Laboratory (Bar Harbor, ME, USA). All animals were maintained under standard laboratory conditions with a 12 h/12 h light/dark cycle with access to food and water ad libitum. The 5xFAD mice were genotyped by polymerase chain reaction analysis of DNA obtained from tail biopsies.

In a first set of experiments, we assessed whether GlyCEST could detect regional differences in glycine concentrations. Nine C57BL/6 WT mice were used for these GlyCEST measurements. Mice were anesthetized using isoflurane (induction with 3%–4%, followed by 1.2%–1.5% maintenance) mixed with 30 : 70 O_2 : N_2O at 2 L/min and placed into the MRI scanner using head fixation with ear and tooth bars. The rectal temperature of the animal was maintained at 37 ± 0.5°C using a custom-made temperature-controlled air conditioning system. After MRI measurements, brains were harvested to correlate the MRI data with biochemical measurements. The extracted brains were cut into 4 mm thick coronal slices (±2 mm from the center of the MR imaging slab) and divided into the cortex and the thalamus.

In a second set examining the reproducibility of GlyCEST data, we measured GlyCEST twice on the same day in the same mice. Five C57BL/6 WT mice were used for these reproducibility measurements.

In a third set, we assessed GlyCEST effects in 5xFAD mice ($n = 7$) and C57BL/6 WT mice ($n = 7$). The GlyCEST measurements and brain sample preparation protocols were identical to those used in the first set of experiments.

2.3. HPLC Glycine Measurements. The specimens extracted from murine brains were measured using HPLC. The collected tissue samples were dissolved in 5 mL of 80% methanol. The samples were centrifuged (3,000 rpm for 15 min), and 5 μL of the supernatant was analyzed by HPLC. The measurement was performed using an Agilent 1100 series HPLC-FLD system (Agilent Technologies, Wilmington, USA) with a fluorescence detector and an Agilent Poroshell 120 EC-C18 (3.0 × 150 mm, 2.7 μm) column. To 5 μL of each sample, 5 μL of boric acid solution, 0.5 μL of ortho-phthalaldehyde/3-mercaptopropionic acid solution, and 0.5 μL of 9-fluorenylmethyl chloroformate solution were added and mixed. For sample injection, Na_2HPO_4 (5 mM, pH 7.6) was used as the mobile phase, and the pump flow rate was set to 0.5 mL/min with a column temperature of 40°C [19]. The Agilent "ChemStation" software (ChemStation for LC 3D systems, Rev B.04.02 SP1) was used to control the system and analyze the data.

2.4. MRI Measurements. MRI was performed using a 16 cm bore 7-T horizontal magnet (Magnex Scientific, Abingdon, UK) with an Agilent Unity-INOVA-300 system (Agilent Inc., Palo Alto, CA, USA) equipped with an actively shielded gradient. A custom-made volume transmitter and a quadrature surface receiver proton coil set (Takashima Seisakusyo, Hino, Japan) were used for the MRI measurements. The imaging protocol was carried out in the following order: (1) localizers (three planes), (2) T2-weighted spin-echo morphological images (T2WI), and (3) GlyCEST. The total image acquisition time for each mouse was 43 min. GlyCEST imaging consisted of a 418 ms saturation pulse train (consisting of ten 40 ms Gaussian-windowed saturation pulses with a 2 ms interpulse delay) at B1rms = 5 μT, followed by centric ordered snapshot fast low-angle shot (FLASH) acquisition. Other imaging parameters were as follows: slice thickness = 2 mm, flip angle = 20°, matrix = 128 × 64, repetition time (TR) (for FLASH) = 4.37 ms, echo time (TE) = 2.20 ms, total TR = 5,000 ms, and signal averages = 4. Raw CEST images were acquired at varying offset frequencies of saturation pulses, from −5 ppm to 5 ppm (−1,500 Hz to 1,500 Hz on 7-T MRI) with a step size of 60 Hz. To map B0 inhomogeneity, water saturation shift referencing images with 100 ms Hanning windowed saturation pulses at B1rms = 0.5 μT were acquired at saturation offset frequencies ranging from −0.5 ppm to 0.5 ppm for the water peak, with a step size of 6 Hz.

2.5. GlyCEST (%) Computations. In GlyCEST imaging, a saturation pulse that selectively suppresses a specific frequency is applied. The resonance frequency of glycine differs from the water peak by +2.85 ppm. When the irradiation position was +2.85 ppm, glycine was saturated, and the signal intensity of the MR image was reduced due to the proton exchange between water and glycine molecules. From the signal intensities of $M_{+2.85\,\mathrm{ppm}}$ and $M_{-2.85\,\mathrm{ppm}}$ at + 2.85 ppm and −2.85 ppm, GlyCEST (%) = $(M_{-2.85\,\mathrm{ppm}} - M_{+2.85\,\mathrm{ppm}})/M_{-2.85\,\mathrm{ppm}} \times 100$ was calculated as an index to quantitatively evaluate the CEST effect. The calculation of GlyCEST (%) on a pixel-by-pixel basis created the glycine concentration map (GlyCEST map). All data processing and analyses were performed using MATLAB (Version 2020a, MathWorks, Natick, MA, USA). Region of interest (ROI) analysis of the GlyCEST map utilized ImageJ software (Version 1.53a, National Institutes of Health, https://imagej.nih.gov/ij/index.html). Five circular ROIs, corresponding to tubes containing 0, 2.5, 5.0, 7.5, and 10.0 mM glycine, were used for the glycine phantom. Four anatomical ROIs, corresponding to the whole cortex, parietal cortex, temporal cortex, and thalamus, were manually drawn on the images of the mouse brain.

2.6. Statistical Analyses. Statistical analysis was performed using GraphPad Prism version 9 (GraphPad Software, La Jolla, CA, USA). Pearson's product-rate correlation coefficient was used to analyze the correlation between glycine concentrations and GlyCEST (%) and between HPLC and GlyCEST data. The paired *t*-test was used to compare the means of glycine concentrations and GlyCEST (%) values in the cortex and thalamus in C57BL/6 WT mice. To evaluate the reproducibility of GlyCEST measurements, we calculated the intraclass correlation coefficient (ICC) [20] between the first and second MRI measurements of GlyCEST (%) values in the cerebral cortex and thalamus of the same C57BL/6 mice. ICC quality was judged as follows: ICC < 0.4 poor, 0.40–0.60 fair, 0.60–0.75 good, and 0.75–1 excellent [21]. The unpaired *t*-test was used to compare the means of regional GlyCEST measurements in WT and 5xFAD mice. A $P < 0.05$ was considered statistically significant. All data are shown as mean ± standard deviation.

3. Results

3.1. Correlation between GlyCEST (%) and Glycine Concentrations. The z-spectra, giving the ratios of water signal intensities with (M_{sat}) and without (M_0) selective saturation, showed that the M_{sat}/M_0 ratio decreased with glycine concentrations increasing from 0 to 10.0 mM (Figure 1(a)). The z-spectra showed an asymmetry between the positive and negative saturation offsets from the water resonance; the CEST asymmetry in each saturation offset was evaluated by the same computation as used for obtaining GlyCEST (%) (Figure 1(b)). The CEST asymmetry increased with increasing glycine concentrations. For each pixel, GlyCEST (%) at the saturation frequency of 2.85 ppm was calculated, and a GlyCEST map was created (Figure 2(a)). GlyCEST (%) increased linearly with increasing glycine concentrations and was significantly correlated with the glycine concentration ($R^2 = 0.99$ and $P < 0.0001$) (Figure 2(b)).

3.2. Correlation between GlyCEST (%) and Glycine Concentrations Determined by HPLC. WT mice ($n = 9$) were imaged for GlyCEST, and ROIs were placed in the cortex and thalamus based on the corresponding regions on T2WI images (Figure 3(a)). Following GlyCEST imaging, the cortex and thalamus of the murine brains were extracted for HPLC analyses. The GlyCEST (%) values were significantly higher in the thalamus than in the cortex ($P < 0.0001$) (Figure 3(b)), which is consistent with the glycine concentrations measured by HPLC (Figure 3(c)). This finding indicates that GlyCEST can detect local differences in cerebral glycine concentrations.

Some WT mice ($n = 5$) were imaged twice for GlyCEST (Supplementary Figure S-1(a)), and ROIs were placed in the cerebral cortex and thalamus (Supplementary Figure S-1(b)). Both cortical and thalamic GlyCEST (%) values showed excellent ICCs (0.88 in both the cortex and the thalamus) (Supplementary Table S-1). These results indicate that GlyCEST measurements are reliable.

3.3. Regional GlyCEST Effects. Next, we imaged GlyCEST in WT ($n = 7$) and 5xFAD ($n = 7$) mice. Figure 4(a) shows representative GlyCEST maps in WT (upper right panel) and 5xFAD (lower right panel) mice. The GlyCEST effects in 5xFAD mice were lower in both the cortex and the thalamus

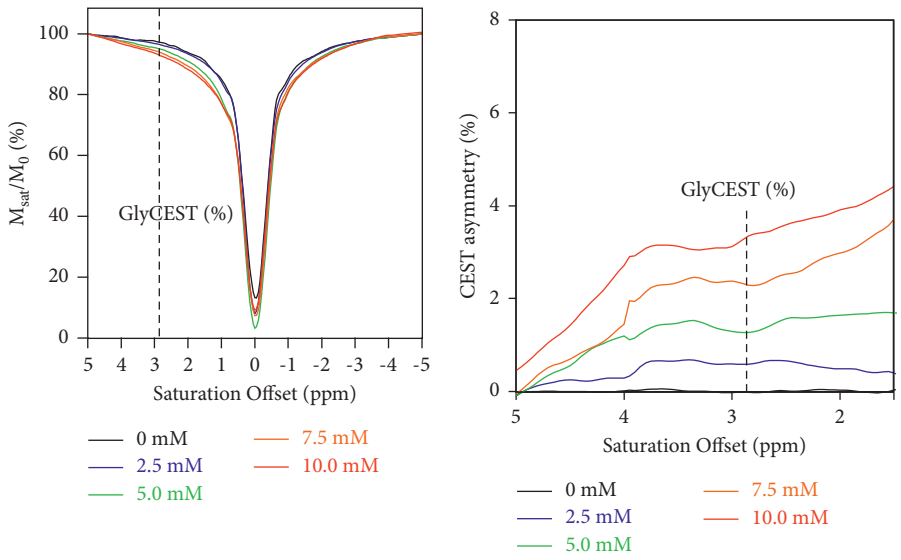

(a) (b)

Figure 1: GlyCEST effects. (a) z-spectra of a phantom containing different glycine concentrations (pH 7.0). (b) CEST asymmetry at various saturation offsets for different glycine concentrations. The same computation was used to determine GlyCEST (%).

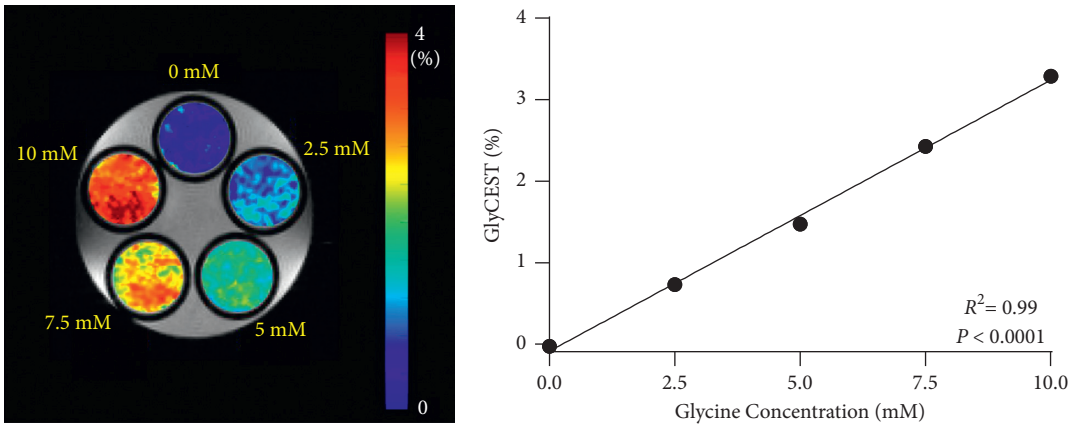

(a) (b)

Figure 2: (a) GlyCEST map of a phantom. (b) Significant linear correlation between GlyCEST (%) and glycine concentration.

compared to those in WT mice. In subregion analyses, GlyCEST (%) was significantly lower in the parietal cortex ($P = 0.0282$, Figure 4(b)), temporal cortex ($P = 0.0020$, Figure 4(c)), and thalamus ($P < 0.0001$, Figure 4(d)) of 5xFAD mice compared to WT animals. No differences were observed in the hippocampus (Figure 4(e)).

Figure 5 shows the relationship between HPLC-determined glycine concentrations and GlyCEST (%) values in the brains of WT and 5xFAD mice. GlyCEST (%) was significantly correlated with the glycine concentration measured by HPLC ($R^2 = 0.4854$ and $P < 0.0001$).

4. Discussion

Amino acid residues, such as –NH, $–NH_2$, and –OH groups, exchange protons with the surrounding water molecules. By applying selective saturation pulses, it is possible to detect specific molecules within tissues, such as sugars, amino acids, transmitters, and nucleosides. While various imaging and application examples of endogenous substances, including APT CEST [22–24] and GluCEST [25, 26], have been reported, CEST imaging of glycine has not yet been described. Because glycine has a high chemical exchange rate with free water [27], a high saturation power in a short pulse time is required to image GlyCEST. High-power saturation pulses increase the specific absorption ratio (SAR) and may impose a high load on the MRI system, resulting in system limitations. In this study, a train of 10 Gaussian pulses, instead of a continuous wave pulse, was applied for presaturation to reduce the load on the radiofrequency (RF) amplifier system [28]. Through this strategy, high-power irradiation could be performed as long as the RF system allowed for it.

The GlyCEST effect of the thalamus was higher than that of the cortex in C57BL/6 WT mice. This result was confirmed

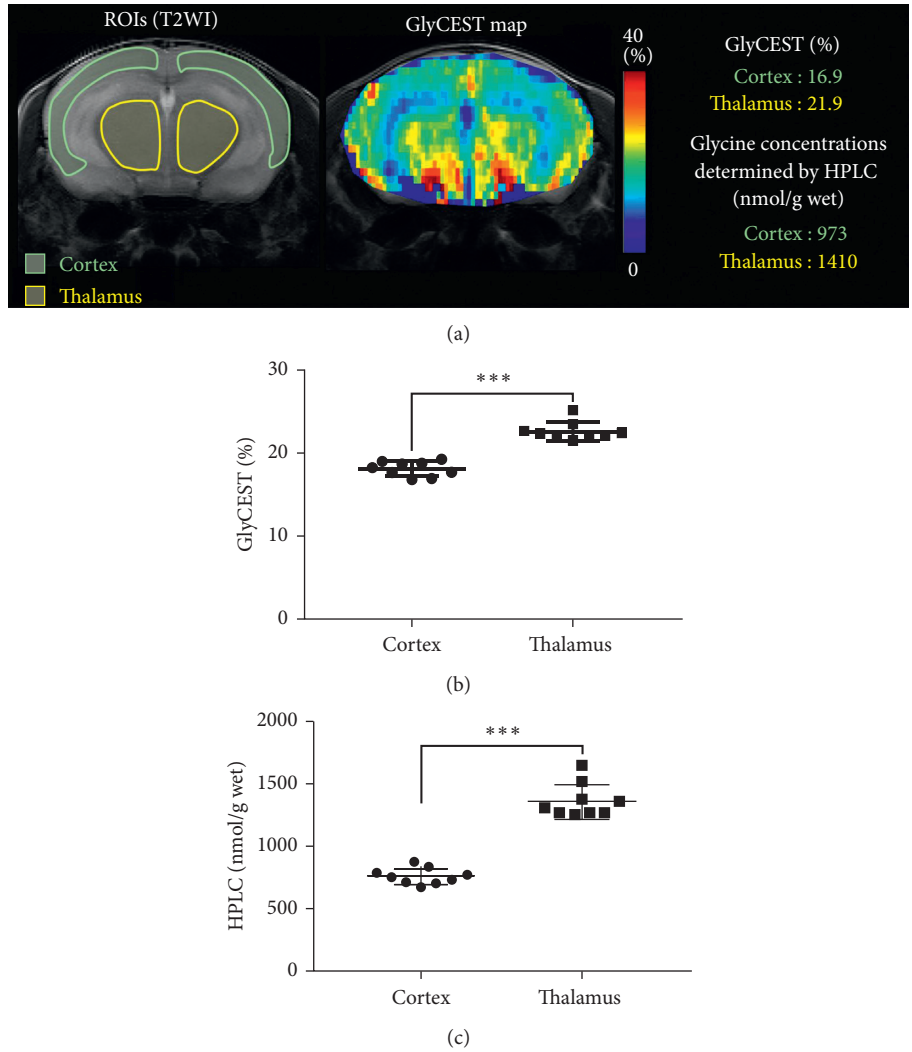

Figure 3: GlyCEST effects and glycine concentrations in C57BL/6 wild-type (WT) mice ($n = 9$). (a) T2-weighted spin-echo image (T2WI) showing regions of interest (ROIs) in a coronal brain slice (left panel) and the corresponding GlyCEST map (center panel). The corresponding GlyCEST (%) and glycine concentrations detected by high-performance liquid chromatography (HPLC) analysis in the cortex and thalamus are also shown (right panel). (b) GlyCEST (%) in the cortex and thalamus measured in T2WI-defined ROIs. (c) Glycine concentrations in the cortex and thalamus detected by HPLC. In both GlyCEST and HPLC measurements, the glycine concentration in the thalamus is higher than that in the cortex. Data were analyzed using the paired t-test ($^{***}P < 0.0001$).

by HPLC measurements. In addition, the GlyCEST maps obtained in this study were in good agreement with the findings of a previous histopathology study that examined bacterial artificial chromosome transgenic mice specifically expressing enhanced green fluorescent protein under the control of the glycine transporter 2 promoter [29].

The pathogenesis of AD has not yet been elucidated; however, the amyloid hypothesis is widely accepted [30]. This hypothesis suggests that the pathological process of AD starts with the abnormal accumulation of amyloid beta (Aβ), followed by the accumulation of tau protein, ultimately leading to neuronal death. However, in AD patients, abnormal protein accumulation does not necessarily correlate spatially and temporally with the pathology, and synaptic deficits appear at the earliest stage [31]. The NMDA receptor is a channel that controls the influx of calcium ions, and channel opening requires the binding of glycine and glutamate. A study using postmortem brain specimens from patients with AD reported that glycine levels were decreased in the superior frontal gyri of AD patients compared to those of healthy subjects [10]. In the present study, the GlyCEST effect was lower in the parietal cortex, temporal cortex, and thalamus of 5xFAD mice, supporting the findings of the previous study. Aβ aggregation increases NMDA receptor activity and induces excitotoxicity [32]. Therefore, it may suppress long-term potentiation and cause cognitive impairment [33, 34]. The cause of cortical and thalamic glycine depletion in 5xFAD mice is still unclear. However, excitotoxicity due to activation of extrasynaptic NMDA receptors may be involved [35]. NMDA receptors exist in both intrasynaptic and extrasynaptic regions of neurons. Intrasynaptic NMDA receptors regulate neural functions.

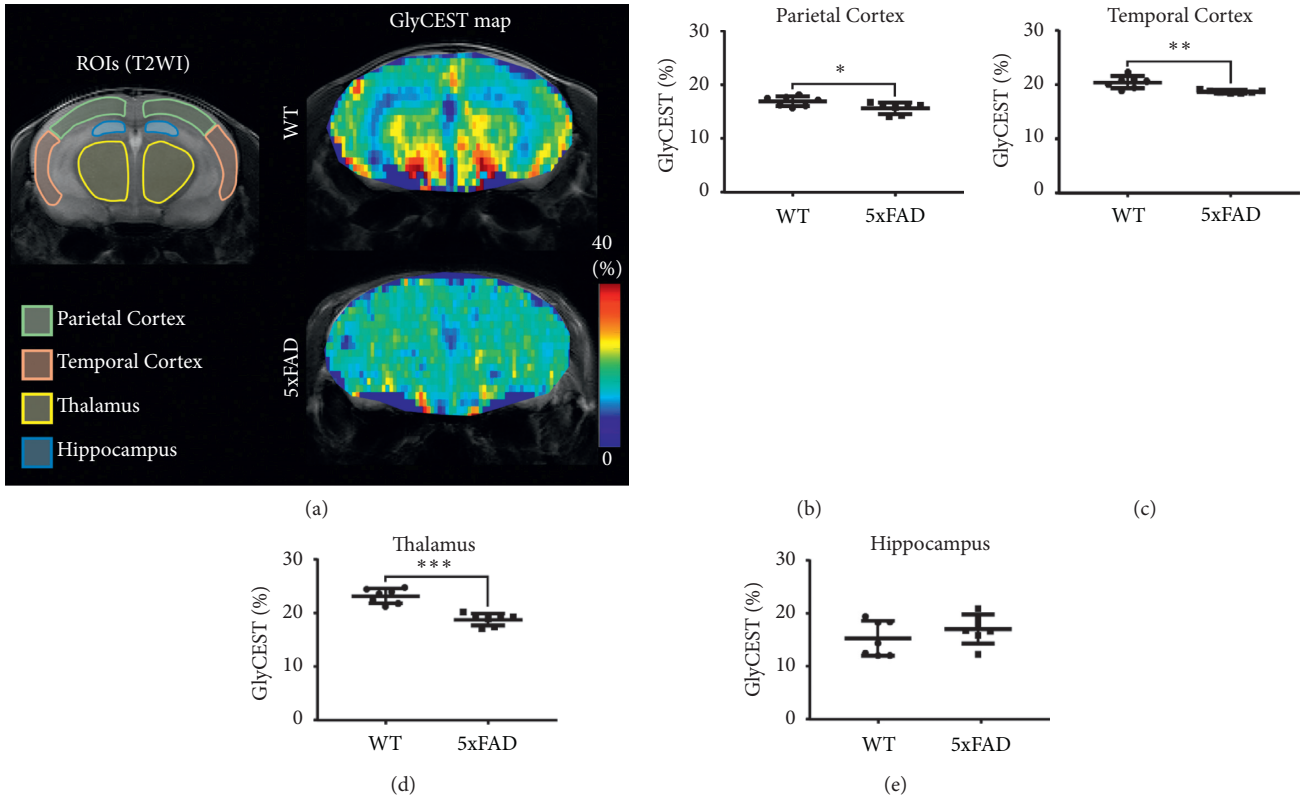

FIGURE 4: GlyCEST effects in WT ($n = 7$) and 5xFAD ($n = 7$) mice. (a) T2WI ROIs in a coronal brain slice (left panel) and the corresponding GlyCEST maps (right panel). (b–e) GlyCEST (%) of the parietal and temporal cortex, thalamus, and hippocampus. Data were analyzed using the unpaired t-test. $^{*}P < 0.05$, $^{**}P < 0.005$, and $^{***}P < 0.0001$.

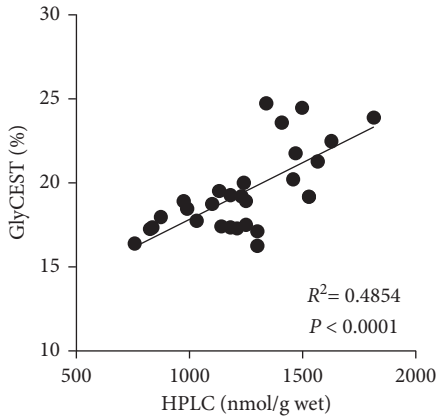

FIGURE 5: Correlation between HPLC and GlyCEST measurements. GlyCEST (%) is significantly correlated with the glycine concentration measured by HPLC.

However, increased activity of extrasynaptic NMDA receptors is thought to induce neuronal death due to excitotoxicity. Memantine, which ameliorates cognitive symptoms in patients with AD, is thought to exert its effects by suppressing the activity of extrasynaptic NMDA receptors [36]. Similar to glycine, D-serine is a small molecule that binds to the glycine binding sites of NMDA receptors, thereby putting NMDA receptors in a state of readiness for activation. Aβ peptides promote synthesis and release of D-serine in astrocytes through serine racemase activation. Moreover, increases in reactive astrocytes due to inflammatory responses may further upregulate D-serine synthesis [37]. Excessive D-serine release may lead to excitotoxicity by activating extrasynaptic NMDA receptors, resulting in synaptic loss and even a decrease in glycine concentration due to neural loss [38, 39]. On the other hand, the biosynthesis of glycine is maintained in equilibrium with L-serine by serine hydroxymethyl-transferase [40]. Increased activity of serine racemase by Aβ may lead to synthesis of D-serine from L-serine, resulting in decreases in both L-serine and glycine levels. On the other hand, the GlyCEST effect in the hippocampus did not differ between WT and 5xFAD mice, which is in concordance with the findings of a study in humans [41]. However, it remains unclear why the hippocampus retains glycine levels in 5xFAD mice. Our group recently reported that the dendrite/axon density of 5xFAD mice is decreased in the cortex but not in the hippocampus [26]. Similarly, a histopathological study found that in 5xFAD mice, the neuronal density of layer 5 was decreased in the cortex but retained in the hippocampus [42]. These regional differences may influence the distribution of glycine concentrations.

The present study has several limitations. The GlyCEST effect determined in this study may have some confounding factors when assessing the cerebral glycine concentration. The GlyCEST effect is pH-dependent and is enhanced under

acidic conditions [27]. Other brain metabolites, magnetization transfer [43] and nuclear Overhauser enhancement [44], may also modulate GlyCEST effects. However, we confirmed the linear correlation of the GlyCEST effect with the glycine concentration using a phantom, and biochemical tests were also performed to confirm the validity of the GlyCEST method.

5. Conclusion

In this study, the CEST-MRI technology was proposed to map the glycine concentration distribution in the murine brain. The results demonstrated that GlyCEST imaging can quantitatively measure glycine concentrations in the brain. The GlyCEST data obtained in C57BL/6 mice showed in good agreement with the biochemical measurements that the glycine concentration in the thalamus was higher than that in the cortex. In 5xFAD mice, an animal model of AD, GlyCEST effects in the cerebral cortex and thalamus, but not in the hippocampus, were lower than those in WT mice. The present method provides a novel *in vivo* imaging tool for researchers to capture the changes in glycine concentrations.

Data Availability

Data and program scripts used to support the findings of this study are available from the corresponding author upon reasonable request.

Conflicts of Interest

The authors declare that there are no conflicts of interest regarding the publication of this study.

Acknowledgments

This work was supported by JSPS KAKENHI (Grant nos. 18K02762B and 20K16774).

Supplementary Materials

The supplementary materials present reproducibility assessments of GlyCEST measurements. Supplementary Figure S-1: GlyCEST maps and GlyCEST (%) in the cortex and thalamus from two measurements. (a) GlyCEST maps of five C57BL/6 mice (A–E). (b) The open and closed circles indicate the GlyCEST (%) average of two measurements in the cortex and thalamus, respectively. Supplementary Table S-1: GlyCEST (%) in the cortex and thalamus from two measurements and their intraclass correlation coefficients (ICCs). (*Supplementary Materials*)

References

[1] J. M. Hopkin and M. J. Neal, "The release of ^{14}C-glycine from electrically stimulated rat spinal cord slices," *British Journal of Pharmacology*, vol. 40, no. 1, pp. 136P–138P, 1970.

[2] R. P. Shank and M. H. Aprison, "The metabolism *in vivo* of glycine and serine in eight areas of the rat central nervous system," *Journal of Neurochemistry*, vol. 17, no. 10, pp. 1461–1475, 1970.

[3] K. A. Cummings and G. K. Popescu, "Glycine-dependent activation of NMDA receptors," *The Journal of General Physiology*, vol. 145, no. 6, pp. 513–527, 2015.

[4] M. S. Hernandes and L. R. P. Troncone, "Glycine as a neurotransmitter in the forebrain: a short review," *Journal of Neural Transmission*, vol. 116, no. 12, pp. 1551–1560, 2009.

[5] C. M. Gladding and L. A. Raymond, "Mechanisms underlying NMDA receptor synaptic/extrasynaptic distribution and function," *Molecular and Cellular Neuroscience*, vol. 48, no. 4, pp. 308–320, 2011.

[6] S.-T. Li and J.-G. Ju, "Functional roles of synaptic and extrasynaptic NMDA receptors in physiological and pathological neuronal activities," *Current Drug Targets*, vol. 13, no. 2, pp. 207–221, 2012.

[7] A. Yu and A. Y. Lau, "Glutamate and glycine binding to the NMDA receptor," *Structure*, vol. 26, no. 7, pp. 1035–1043, 2018.

[8] F. Zafra, C. Aragon, L. Olivares, N. Danbolt, C. Gimenez, and J. Storm-Mathisen, "Glycine transporters are differentially expressed among CNS cells," *Journal of Neuroscience*, vol. 15, no. 5, pp. 3952–3969, 1995.

[9] J. T. Coyle and G. Tsai, "The NMDA receptor glycine modulatory site: a therapeutic target for improving cognition and reducing negative symptoms in schizophrenia," *Psychopharmacology*, vol. 174, no. 1, pp. 32–38, 2004.

[10] T. Nuzzo, A. Mancini, M. Miroballo et al., "High performance liquid chromatography determination of L-glutamate, L-glutamine and glycine content in brain, cerebrospinal fluid and blood serum of patients affected by Alzheimer's disease," *Amino Acids*, vol. 53, no. 3, pp. 435–449, 2021.

[11] R. González-Domínguez, T. García-Barrera, J. Vitorica, and J. L. Gómez-Ariza, "Region-specific metabolic alterations in the brain of the APP/PS1 transgenic mice of Alzheimer's disease," *Biochimica et Biophysica Acta*, vol. 1842, no. 12, pp. 2395–2402, 2014.

[12] S. F. Graham, C. Holscher, and B. D. Green, "Metabolic signatures of human Alzheimer's disease (AD): 1H NMR analysis of the polar metabolome of post-mortem brain tissue," *Metabolomics*, vol. 10, no. 4, pp. 744–753, 2014.

[13] M. J. Kaufman, A. P. Prescot, D. Ongur et al., "Oral glycine administration increases brain glycine/creatine ratios in men: a proton magnetic resonance spectroscopy study," *Psychiatry Research: Neuroimaging*, vol. 173, no. 2, pp. 143–149, 2009.

[14] C. Choi, S. K. Ganji, R. J. DeBerardinis et al., "Measurement of glycine in the human brain *in vivo* by 1 H-MRS at 3 T: application in brain tumors," *Magnetic Resonance in Medicine*, vol. 66, no. 3, pp. 609–618, 2011.

[15] A. Banerjee, S. Ganji, K. Hulsey et al., "Measurement of glycine in gray and white matter in the human brain in vivo by 1H MRS at 7.0 T," *Magnetic Resonance in Medicine*, vol. 68, no. 2, pp. 325–331, 2012.

[16] G. Liu, X. Song, K. W. Y. Chan, and M. T. McMahon, "Nuts and bolts of chemical exchange saturation transfer MRI," *NMR in Biomedicine*, vol. 26, no. 7, pp. 810–828, 2013.

[17] H. Oakley, S. L. Cole, S. Logan et al., "Intraneuronal β-amyloid aggregates, neurodegeneration, and neuron loss in transgenic mice with five familial Alzheimer's disease mutations: potential factors in amyloid plaque formation," *Journal of Neuroscience*, vol. 26, no. 40, pp. 10129–10140, 2006.

[18] Institute for Laboratory Animal Research, *Guide for the Care and Use of Laboratory Animals*, National Academies Press, 8th edition, Washington (DC), 2011.

[19] J. W. Henderson and A. Brooks, *Improved Amino Acid Methods Using Agilent ZORBAX Eclipse Plus C18 Columns for*

a Variety of Agilent LC Instrumentation and Separation Goals, p. 5990, Agilent Pub, Santa Clara, California, 2010, 4547EN.

[20] T. K. Koo and M. Y. Li, "A guideline of selecting and reporting intraclass correlation coefficients for reliability research," *Journal of Chiropractic Medicine*, vol. 15, no. 2, pp. 155–163, 2016.

[21] D. V. Cicchetti and S. A. Sparrow, "Developing criteria for establishing interrater reliability of specific items: applications to assessment of adaptive behavior," *American Journal of Mental Deficiency*, vol. 86, no. 2, pp. 127–137, 1981.

[22] J. Zhou, J.-F. Payen, D. A. Wilson, R. J. Traystman, and P. C. M. Van Zijl, "Using the amide proton signals of intracellular proteins and peptides to detect pH effects in MRI," *Nature Medicine*, vol. 9, no. 8, pp. 1085–1090, 2003.

[23] C. K. Jones, M. J. Schlosser, P. C. M. Van Zijl, M. G. Pomper, X. Golay, and J. Zhou, "Amide proton transfer imaging of human brain tumors at 3T," *Magnetic Resonance in Medicine*, vol. 56, no. 3, pp. 585–592, 2006.

[24] J. Zhou, J. O. Blakeley, J. Hua et al., "Practical data acquisition method for human brain tumor amide proton transfer (APT) imaging," *Magnetic Resonance in Medicine*, vol. 60, no. 4, pp. 842–849, 2008.

[25] K. Cai, M. Haris, A. Singh et al., "Magnetic resonance imaging of glutamate," *Nature Medicine*, vol. 18, no. 2, pp. 302–306, 2012.

[26] H. Igarashi, S. Ueki, H. Kitaura et al., "Longitudinal GluCEST MRI changes and cerebral blood flow in 5xFAD mice," *Contrast Media & Molecular Imaging*, vol. 2020, Article ID 8831936, 12 pages, 2020.

[27] F. C. Wermter, C. Bock, and W. Dreher, "Investigating GluCEST and its specificity for pH mapping at low temperatures," *NMR in Biomedicine*, vol. 28, no. 11, pp. 1507–1517, 2015.

[28] Z. Zu, K. Li, V. A. Janve, M. D. Does, and D. F. Gochberg, "Optimizing pulsed-chemical exchange saturation transfer imaging sequences," *Magnetic Resonance in Medicine*, vol. 66, no. 4, pp. 1100–1108, 2011.

[29] H. U. Zeilhofer, B. Studler, D. Arabadzisz et al., "Glycinergic neurons expressing enhanced green fluorescent protein in bacterial artificial chromosome transgenic mice," *Journal of Comparative Neurology*, vol. 482, no. 2, pp. 123–141, 2005.

[30] J. Hardy and D. J. Selkoe, "The amyloid hypothesis of Alzheimer's disease: progress and problems on the road to therapeutics," *Science*, vol. 297, no. 5580, pp. 353–356, 2002.

[31] B. D. Boros, K. M. Greathouse, E. G. Gentry et al., "Dendritic spines provide cognitive resilience against Alzheimer's disease," *Annals of Neurology*, vol. 82, no. 4, pp. 602–614, 2017.

[32] Y.-J. Huang, C.-H. Lin, H.-Y. Lane, and G. E. Tsaid, "NMDA neurotransmission dysfunction in behavioral and psychological symptoms of Alzheimer's disease," *Current Neuropharmacology*, vol. 10, no. 3, pp. 272–285, 2012.

[33] G. M. Shankar, B. L. Bloodgood, M. Townsend, D. M. Walsh, D. J. Selkoe, and B. L. Sabatini, "Natural oligomers of the Alzheimer Amyloid-β protein induce reversible synapse loss by modulating an NMDA-type glutamate receptor-dependent signaling pathway," *Journal of Neuroscience*, vol. 27, no. 11, pp. 2866–2875, 2007.

[34] G. Yamin, "NMDA receptor-dependent signaling pathways that underlie amyloid β-protein disruption of LTP in the hippocampus," *Journal of Neuroscience Research*, vol. 87, no. 8, pp. 1729–1736, 2009.

[35] T. Papouin, L. Ladépêche, J. Ruel et al., "Synaptic and extrasynaptic NMDA receptors are gated by different endogenous coagonists," *Cell*, vol. 150, no. 3, pp. 633–646, 2012.

[36] P. Xia, H.-S. V. Chen, D. Zhang, and S. A. Lipton, "Memantine preferentially blocks extrasynaptic over synaptic NMDA receptor currents in hippocampal autapses," *Journal of Neuroscience*, vol. 30, no. 33, pp. 11246–11250, 2010.

[37] Q.-S. Chen, W.-Z. Wei, T. Shimahara, and C.-W. Xie, "Alzheimer amyloid β-peptide inhibits the late phase of long-term potentiation through calcineurin-dependent mechanisms in the hippocampal dentate gyrus," *Neurobiology of Learning and Memory*, vol. 77, no. 3, pp. 354–371, 2002.

[38] M. Talantova, S. Sanz-Blasco, X. Zhang et al., "A β induces astrocytic glutamate release, extrasynaptic NMDA receptor activation, and synaptic loss," *Proceedings of the National Academy of Sciences*, vol. 110, no. 27, pp. E2518–E2527, 2013.

[39] C.-H. Lin, H.-T. Yang, and H.-Y. Lane, "D-glutamate, D-serine, and D-alanine differ in their roles in cognitive decline in patients with Alzheimer's disease or mild cognitive impairment," *Pharmacology Biochemistry and Behavior*, vol. 185, Article ID 172760, 2019.

[40] W. Wang, Z. Wu, Z. Dai, Y. Yang, J. Wang, and G. Wu, "Glycine metabolism in animals and humans: implications for nutrition and health," *Amino Acids*, vol. 45, no. 3, pp. 463–477, 2013.

[41] I. Tarbit, E. K. Perry, R. H. Perry, G. Blessed, and B. E. Tomlinson, "Hippocampal free amino acids in Alzheimer's disease," *Journal of Neurochemistry*, vol. 35, no. 5, pp. 1246–1249, 1980.

[42] S. Jawhar, A. Trawicka, C. Jenneckens, T. A. Bayer, and O. Wirths, "Motor deficits, neuron loss, and reduced anxiety coinciding with axonal degeneration and intraneuronal Aβ aggregation in the 5XFAD mouse model of Alzheimer's disease," *Neurobiology of Aging*, vol. 33, no. 1, pp. 196–240, 2012.

[43] R. M. Henkelman, G. J. Stanisz, and S. J. Graham, "Magnetization transfer in MRI: a review," *NMR in Biomedicine*, vol. 14, no. 2, pp. 57–64, 2001.

[44] C. K. Jones, A. Huang, J. Xu et al., "Nuclear Overhauser enhancement (NOE) imaging in the human brain at 7T," *NeuroImage*, vol. 77, pp. 114–124, 2013.